Solar Phys (2007) 240: 89–105
DOI 10.1007/s11207-006-0203-5

Helical Eruptive Prominence Associated with a Pair of Overlapping CMEs on 21 April 2001

Syed Salman Ali · Wahab Uddin · Ramesh Chandra · D.L. Mary · Bojan Vršnak

Received: 15 April 2006 / Accepted: 12 November 2006 / Published online: 1 March 2007

Abstract The eruption of limb prominence on 21 April 2001 associated with two coronal mass ejections (CMEs) is investigated. Hα images reveal two large-scale eruptions (a prominence body and a southern foot-point arch), both showing helical internal structure. These two eruptions are found to be spatially and temporally associated with the corresponding CMEs. The kinematics and the study of geometrical parameters of the prominence show that the eruption was quite impulsive (with peak acceleration $\approx$470 m s^{-2}) and has taken place for relatively low pitch angle of helical threads, not exceeding $\tan\theta \approx 1.2$. The stability criteria of the prominence are revisited in the light of the model of Vršnak (1990, *Solar Phys.* **129**, 295) and the analysis shows that the eruption violates the instability criteria of that model. Finally, the energy stored in the prominence circuit and the energies (kinetic, potential, and magnetic) of the associated CMEs are estimated and it is found that there was enough energy stored in the prominence to drive the two CMEs.

S.S. Ali is on leave from Aligarh Muslim University, Aligarh, 202 002, India.

S.S. Ali (✉) · W. Uddin · R. Chandra · D.L. Mary
Aryabhatta Research Institute of Observational Sciences, Manora Peak, Naini Tal, 263 129, India
e-mail: salman@aries.ernet.in

W. Uddin
e-mail: wahab@aries.ernet.in

R. Chandra
e-mail: ramesh@aries.ernet.in

Present address:
D.L. Mary
Astronomisches Rechen-Institut, am Zentrum fuer Astronomie, Moenchofstrasse 12-14,
69120 Heidelberg, Germany
e-mail: dmary@aries.ernet.in

B. Vršnak
Hvar Observatory, Faculty of Geodesy, 10000 Zagreb, Croatia
e-mail: bvrsnak@geodet.geof.hr

1. Introduction

It is widely accepted that prominence eruptions are the near-surface activity most often associated with coronal mass ejections (Webb, Krieger, and Rust, 1976; Munro *et al.*, 1979; Webb and Hundhausen, 1987; St. Cyr and Webb, 1991; Gopalswamy *et al.*, 2003). The most probable initial configuration of a coronal mass ejection (CME) is a flux rope, consisting of twisted field lines that form a dark cavity stretched in the corona along the photospheric inversion line (*e.g.*, Low, 1996). Cold and dense prominence material accumulates in the lower parts of helical flux tube, where concave field lines form a magnetic-dip configuration, providing support against gravity (*e.g.*, Priest, Hood, and Anzer, 1989). Coronal cavity is a rather inconvenient feature for observations owing to reduced emission, whereas prominences are easily observed and thus are good tracers of flux ropes in the corona.

Some authors have treated the prominence eruption as a secondary process of the CME phenomenon, since the prominence itself may not have enough energy to drive a CME (Hundhausen, 1999; Smith, Hildner, and Quin, 1992). However, Filippov (1998) has shown that CMEs can be caused by the eruption of inverse polarity prominences. Recently, Maričić *et al.* (2004) showed that the take-off of the prominence and the overlying structure is tightly synchronized, favoring the hypothesis according to which the whole structure erupts as a single entity (Forbes, 2000).

The mechanism of the prominence/CME eruption is not yet fully understood, because the underlying magnetic structure is poorly known. In particular, the prominence is usually very complex itself, and most often it is not possible to disclose its configuration. Moreover, not much is known about the overall magnetic structure within which the prominence is nested. Consequently, a number of mechanisms for the trigger/destabilization of prominences were proposed by various authors (for an overview see Tandberg-Hanssen, 1995), including magnetic reconnection (Priest and Krishnan, 1990), resistive instabilities (Priest, 1985), wave disturbance because of a flare (Uchida, 1974), critical twist configuration (Vršnak, 1988), emerging flux, moving pores, flux cancellation (Schmieder, 1990), and kink instability (Sakurai, 1976). However, most generally, the eruption of the prominence and the associated magnetic structure could be considered as a process of catastrophic loss of equilibrium (*cf.* Forbes, 2000).

One of the most important properties of active prominences is their helical structure. Although the pre-eruptive structure is usually very complex, the helical structure often becomes prominent during the acceleration phase (*e.g.*, Vršnak, Ruždjak, and Rompolt, 1991). Several authors performed case studies of the twist of helical fine structure threads in prominences (Tandberg-Hanssen and Malville, 1974; Engvold, Malville, and Rustad, 1976; House and Berger, 1987; Moore, 1988; Vršnak, 1990a, 1990b, 1990c), following the idea that the Hα threads disclose helical structure of prominence magnetic field. If this assumption is correct, the study of twist is an effective tool for analyzing the structure and stability of prominences and the magnetic arcades in which they are embedded (Sakurai, 1976; van Tend and Kuperus, 1978; Pneuman, 1980; An, 1984; Hood and Anzer, 1987; Vršnak, 1988; Vršnak, Ruždjak, and Rompolt, 1991; Vršnak *et al.*, 1993; Romano, Contarino, and Zuccarello, 2003).

In order to establish criteria for the onset of eruptive instability in prominences, Vršnak (1990c) proposed a model of a uniformly twisted, semi-toroidal prominence anchored at both ends in the photosphere. The model provides the critical value of the twist as a function of the semi-torus aspect ratio. A prominence with twist smaller than critical is bound to be stable. Measurements performed by Vršnak, Ruždjak, and Rompolt (1991) and Romano, Contarino, and Zuccarello (2003) seemingly supported the model results by Vršnak (1990c).

In the present paper we test the stability criteria of Vršnak (1990c) for the prominence eruption. For this purpose we analyze the prominence that erupted on the east limb on 21 April 2001. The eruptive prominence exposed a helical-like pattern, suitable to carry out such a study. We also explore the spatial and temporal association between the prominence eruption and the two associated CMEs, as well as their energetics.

2. Observations

To carry out the present study, we have used Hα data taken from the 15 cm, f/15 Coudé refractor equipped with the CCD Photometric Camera (12 bit, 512×512 pixel, pixel size = 15 μm^2) and the Bernhard Halle Hα (6563 Å/0.5 Å) filter. With the help of a Barlow lens, the image has been magnified twice, to get a resolution of 0.65″ per pixel. Further details are available in Joshi, Chandra, and Uddin (2003).

The prominence eruption was also observed by the Extreme-ultraviolet Imaging Telescope onboard the Solar and Heliospheric Observatory (SOHO/EIT 195 Å), which has a 45×45 arcmin field of view and spatial resolution of 2.6″ per pixel (Delaboudiniere *et al.*, 1995). The associated CMEs have been observed by the Large Angle and Spectrometric Coronagraph onboard SOHO (SOHO/LASCO; Brueckner *et al.*, 1995) in the field of view of C2 and C3 instruments. The fields of view of the C2 and C3 coronagraphs extend from $2R_\odot$ to $6R_\odot$ and from $4R_\odot$ to $30R_\odot$, respectively.

3. Morphology and Kinematics

3.1. Chronology of Events

We summarize the chronology of the events in Table 1 and illustrate the most important developments in Figure 1, which includes selected Hα filtergrams of prominence eruption along with the EIT 195 Å difference images and the white light LASCO C2 and C3 images.

Table 1 Chronology of events.

07:50:47	Prominence activation and slow rise
07:55:27	Acceleration maximum (470 $m\,s^{-2}$)
07:58:48	Multiple foot-point structure became recognizable
08:03:32	Multiple foot-point structure simplified
08:03:32	Acceleration dropped to zero (at $\approx 1.02 \times 10^5$ km)
08:06 onwards	Progressing eruption with well-defined helical structure
08:15:22	Northern foot-point straightened ("detwisting")
08:16:06	Eruption seen in the EIT 195 Å field of view
08:20:52	Major kink developed in the southern arch
08:20:53	Arch at the southern foot-point swelled and started to rise
08:21:53	First CME appeared in the LASCO C2 field of view
08:43:00	Southern arch erupted
09:05:28	Second CME appeared in the LASCO C2 field of view

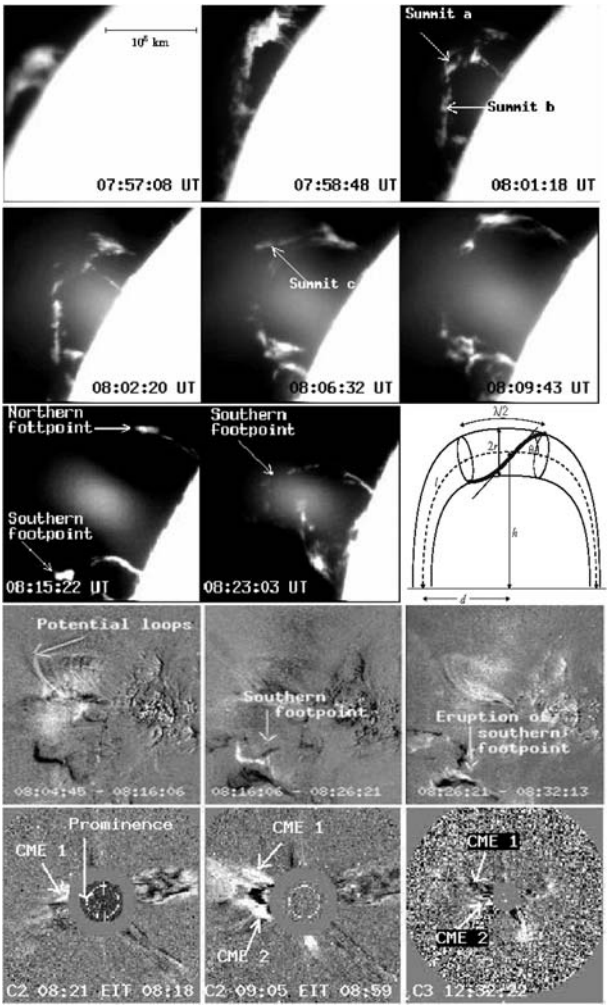

Figure 1 Evolution of the Hα prominence (upper three rows; $333'' \times 333''$), the sketch of helical structure of the prominence (extreme right, third row from top), prominence eruption in the EIT 195 Å difference images (fourth row from top; $767'' \times 826''$), and LASCO C2 and C3 images (bottom row). North is up; west is right.

3.2. Spatial and Temporal Correlation

The spatial correlation between prominence and the two associated CMEs can be understood with the help of Hα filtergrams, EIT 195 Å difference images, and LASCO observations of CMEs (Figure 1). The comparison of the location of the prominence eruption with the position angle of CMEs suggests that these events are spatially correlated. Moreover, the composed LASCO/C2 – EIT image (bottom left panel of Figure 1) shows the EIT erupting prominence below the advancing CME, thus confirming that these events are spatially correlated.

In Figure 2 the height – time profiles of the leading edge of the prominence and the leading edges of the two associated CMEs are plotted. At 07:50:47 UT the prominence was at $1.02R_{\odot}$, whereas the back-extrapolation of the first CME intersects $1.0R_{\odot}$ at 07:50 UT. The plot reveals strong temporal association between the prominence eruption and the first CME. The position angle of the second CME (not included in the LASCO CME catalog) and the position angle of the eruption of the arch-segment at the southern foot-point of the

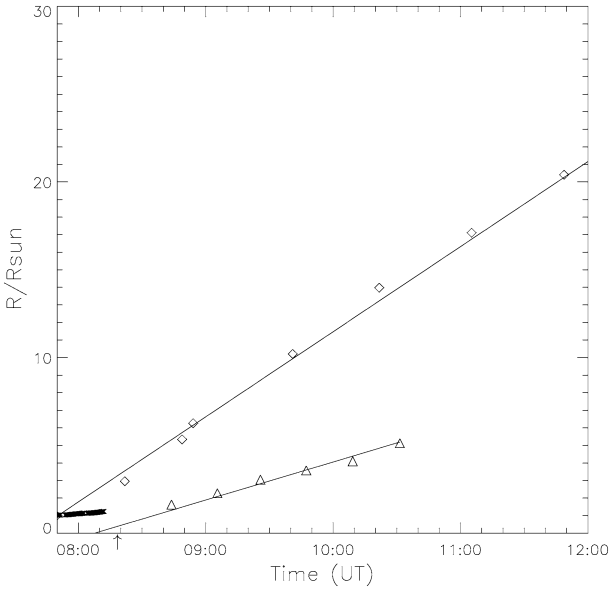

Figure 2 The height – time profiles of the first CME (◇), the second CME (△), and the prominence (×). The arrow indicates the time of the eruption of the southern foot-point arch.

prominence (see Section 3.1 and Figure 1) suggest that they are spatially correlated. The Hα eruption was too large to be entirely kept within the field of view. Hence, the eruption of the southern foot-point could not be covered properly and we could not plot the height – time profile of its rise. However, the information we could gather from our data suggests that the second CME and the eruption of southern foot-point are associated to within ± 10 minutes.

3.3. Prominence Kinematics

The smoothed height – time profile (for details of the procedure see the Appendix) of the leading edge of the prominence, along with the velocity and acceleration profiles, are presented in Figure 3. The plots reveal that destabilization of the prominence started before 07:50:47 UT, since at this time the ascending motion was already characterized by the velocity of 20 ± 3 km s^{-1}, which was observed for about 1.5 min. Thereafter, the prominence velocity started to increase with an average acceleration of 259 m s^{-2}. The acceleration maximum of 470 ± 70 m s^{-2} was attained at around 07:55:27 UT (272 ± 5 s after 07:50:47 UT), at a height of $1.04 R_{\odot}$. At this stage the prominence velocity was 90 km s^{-1}. After that the acceleration continuously decreases. At around 08:03:32 UT, at a height of $1.14 R_{\odot}$, the acceleration dropped to zero. So, the acceleration phase lasted for about 10 min. After the velocity attained its maximum, it remained approximately constant at a value of 161 ± 8 km s^{-1}.

4. Evolution of Geometrical Parameters

An important factor related to the stability of the prominence and the dynamics of the eruption is the twist of magnetic field. We have used the Hα images to measure the pitch angle of helical patterns, θ, assuming that the prominence is a semi-toroidal flux rope anchored at both ends in the photosphere.

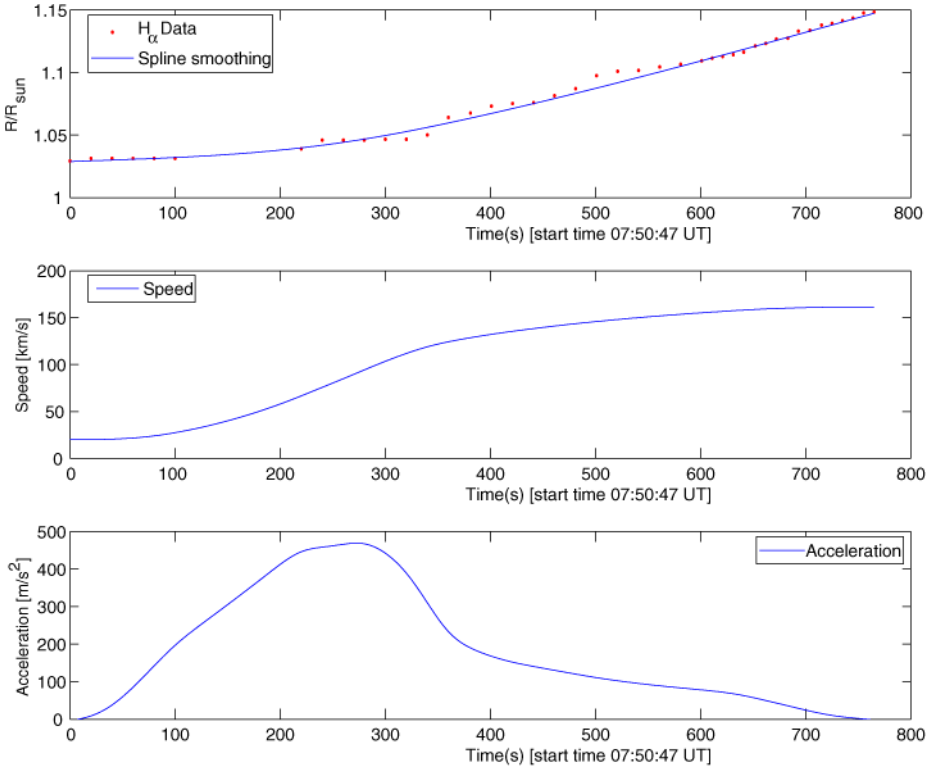

Figure 3 The smoothed height – time profile and raw Hα data (dots), velocity profile, and acceleration profile of the prominence (from top to bottom).

The pitch angle of a particular thread was estimated independently by direct measurement, as well as by measuring the pitch length (λ) and the radius (r) of the helix, where these quantities are related as

$$\tan\theta = X = 2\pi r/\lambda. \tag{1}$$

We have measured the pitch angle at three positions (denoted as a, b, and c in Figure 1) along the prominence axis close to its summit. Since measurements of the pitch angle θ during the eruptive phase of the prominence are difficult to make because of fast changes of the prominence body, the measurements were repeated several times and an average value was obtained. A typical error amounts to $\pm 5^\circ$. The helical patterns used for the measurements are marked in Figure 4 at the beginning and near the end of the time intervals for which the variation of pitch angles is measured for summit segments a, b, and c, respectively.

Figure 5 shows the temporal variation of the radius r and pitch length λ of prominence threads at segments a, b, and c. It can be seen from Figure 5 that the radius decreased at segments a and c (at a, from 10 200 km to 8 300 km; at c, from 7 800 km to 3 900 km), whereas the pitch length increased simultaneously at the same locations (at a, from 66 300 km to 78 000 km; and at c from 90 600 km to 122 800 km). At the summit segment b, the radius and the pitch length stayed roughly constant at 6 300 km and 34 100 km, respectively. The decrease of radius and increase of pitch length at segments a and c reveal the stretching of

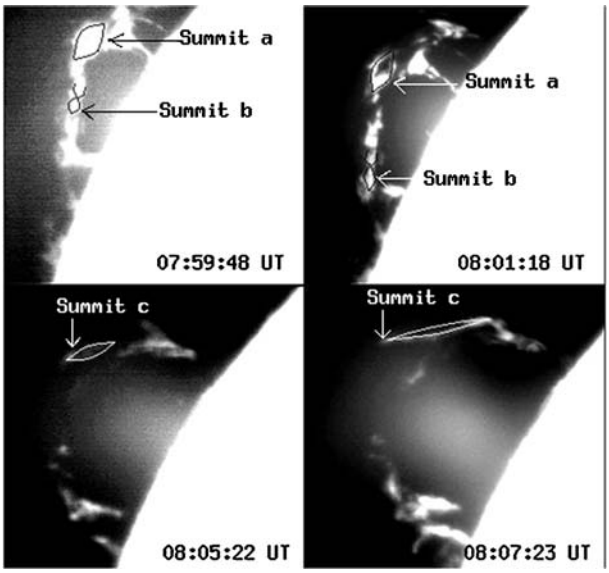

Figure 4 The sketch of threads identified for the measurement of pitch angles at summit segments a, b, and c, respectively. The filtergrams presented are those at the beginning and end of the corresponding time intervals.

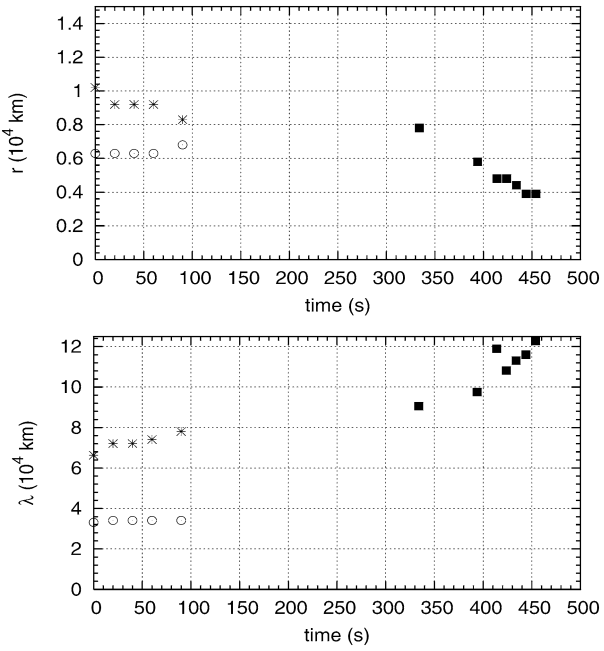

Figure 5 The variation of the radius of the flux tube (top panel) and pitch length (λ) (bottom panel) with time (start time 07:59:48 UT), at the summit segments a (⁎), b (⊙), and c (■).

prominence body at these locations. The temporal variation of the parameter $X = \tan\theta$ is shown in the top panel of Figure 6, where it exposes a decreasing trend.

There are two important constraints imposed by the fact that the magnetic field lines are anchored in the photosphere (Vršnak, Ruždjak, and Rompolt, 1991). First, in the absence of diffusion, the flux of the longitudinal component of the magnetic field must remain constant

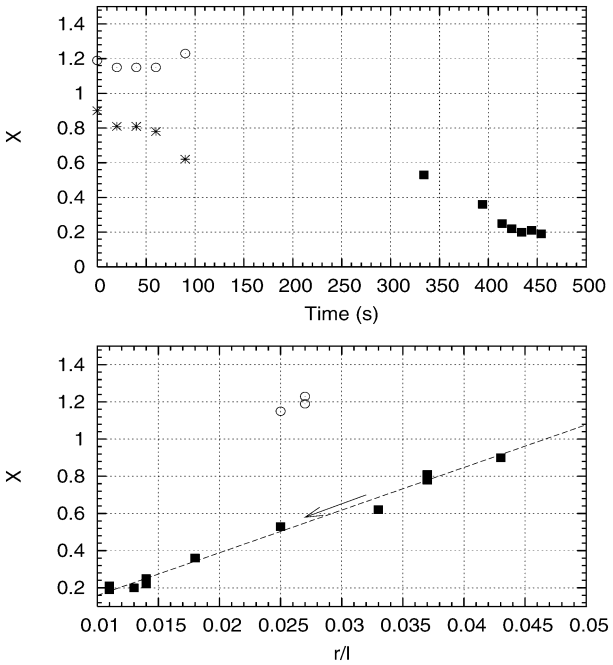

Figure 6 The variation of the pitch angle (expressed as $X = \tan\theta$) with time (top panel; start time 07:59:48 UT) at segments a (∗), b (⊙), and c (■), and the dependence of the pitch angle on the ratio r/l (bottom panel), at segment b (⊙) and at segments a and c (■). The arrow indicates the time development.

along the axis of the tube, and second, in the absence of magnetic reconnection within the tube, the total twist of a field line (Φ) must be conserved.[1] For the uniform twist configuration, the conservation of twist for a thread of the total length l implies

$$\Phi = lX/r = \text{const}, \tag{2}$$

which is equivalent to the conservation of the azimuthal flux in the tube.

In Figure 6 (bottom panel) we have plotted the dependence of X on the ratio r/l. The graph reveals a linear dependence $X \propto r/l$ for segments a and c, indicating that the azimuthal flux remains constant within the flux tube. This implies that no reconnection took place inside the flux tube.

At $\approx$08 UT, when the first set of the pitch angle measurements were performed, the parameter X amounted to about 0.8 and 1.2 at segments a and b, respectively. At this time, the ratio of the height and foot-point semi-distance, $Z = h/d$, amounted to $Z = 0.9 - 0.98$. Placing these data points (Figure 7, top panel) into the $X - Z$ plane of the Vršnak model and comparing the result with Figure 3a of Vršnak (1990c), we find that they fall into the stability region of the graph. In Vršnak (1990c) the "instability curve" of the smallest X at $Z = 0.9$ is curve 1, and at this height the prominence is unstable if $X > 1.6$. In contrast, for the case $X = 1.2$, the lowest height at which the instability should occur is $Z \approx 1.2$ (curve 3), *i.e.*, the prominence should be some 30% higher. Moreover, extrapolating the data points in Figure 7 (top panel) backwards using the assumption of constant twist (which is also supported by Figure 6), *i.e.*, $X \propto Z^{-1}$, shows that the pitch angle fell in the stable region of the $X - Z$ plane also at earlier stages of eruption.

[1] Note that the twist of the field lines around the tube axis could partly transform into a wriggle if the prominence writhes strongly out of the plane.

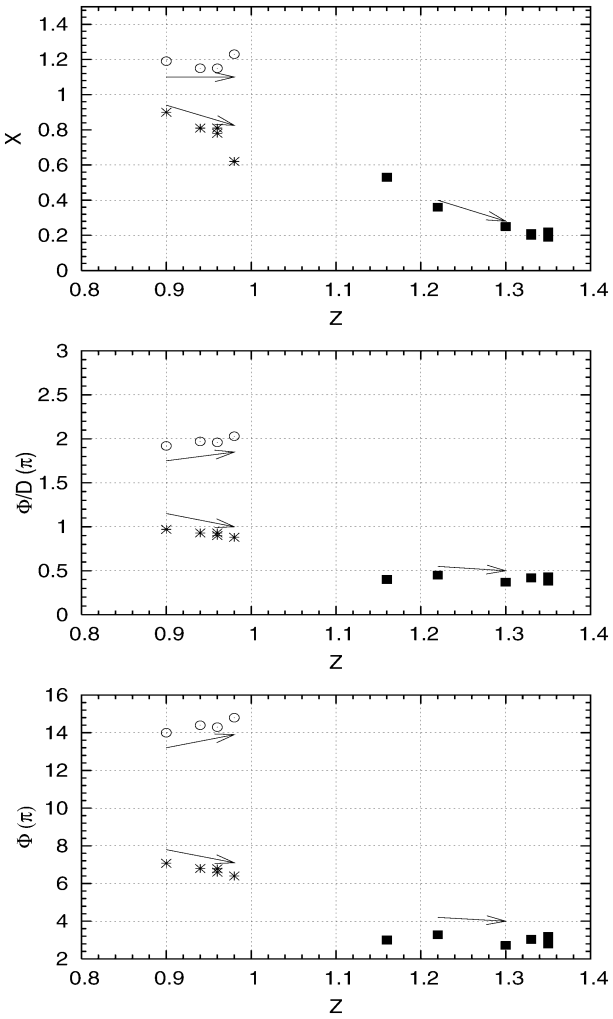

Figure 7 Variation of the parameter X (top panel), Φ (middle panel), and Φ/D (bottom panel) with Z, at summit segments a ($*$), b ($\odot$), and c ($\blacksquare$). The arrows indicate the time development.

In the middle and bottom panels of Figure 7 we show the evolution of the parameter $\Phi/D = lX/d$ (middle panel) and Φ (bottom panel) as a function of the normalized height $Z = h/d$, where $D = d/r$ is the foot-point half-separation expressed in the units of the prominence radius r (Vršnak, 1988). Here, $d = 75\,075$ km and $r = 10\,237$ km. Comparing our middle and bottom panels of Figure 7 with the model results shown in Figures 3b and 3c of Vršnak (1990c), we find that the segment b data lie in the region populated by most of the instability lines. According to the model, this region should correspond to the onset of the instability. However, at this time the acceleration phase was almost over (see Table 1 and Figure 3).

The model predicts that, for the eruptive instability to set in, the magnetic field should become sufficiently twisted and the prominence should surpass a critical height. In this respect, we note that the most direct observational quantity is the pitch angle θ, *i.e.*, $X = \tan\theta$, whereas other parameters rely on additional assumptions. According to Vršnak (1990c), the critical value of X should be larger than $\approx 1.6-2$ at $(Z)_{\rm crit} = 0.8-1$. It was also suggested

therein that the prominences not attaining these critical values should remain stable and hence should not erupt. In a recent case study, Romano, Contarino, and Zuccarello (2003) measured the prominence twist using TRACE images and found agreement with the empirical results of (Vršnak, Ruždjak, and Rompolt, 1991) and the model by Vršnak (1990c). However, our observations apparently do not support the model by Vršnak (1990c), since the parameter X did not show values that fall into the instability region of the model results.

5. Energetics

An important aspect of the relationship between erupting prominences and coronal mass ejections is the energy stored in the prominence and the energy carried out by CME. The eruption of 21 April 2001 provides a good opportunity to have a look into this problem. In the following, we try to estimate the energy stored in the prominence and compare it with the energy of both the associated CMEs.

5.1. Energy of Prominence

The calculation of the energy of the prominence is carried out following the model of Martens (1986). Most of the prominence parameters are directly derived from Hα filtergrams.

We consider the prominence as a line current of strength I, located at the height h, above the magnetic neutral line. The Kuperus and Raadu (1974) model is used to describe the electric circuit. The interaction between the prominence and the background magnetic field determines the dynamical behaviour of the prominence. The momentum equation of an active prominence in Gaussian units is given by Martens and Kuin (1989):

$$m\frac{\mathrm{d}^2h}{\mathrm{d}t^2} = \frac{lI^2}{c^2h} - \frac{lIB}{c} - \frac{mg_sR_s^2}{(R_s+h)^2}, \tag{3}$$

where R_s is the solar radius, g_s is the gravitational acceleration at the solar surface, and B is the background magnetic field, which is supposed to be potential. Following Tang *et al.* (1999) and Wu *et al.* (2002) we take

$$B = B_0\mathrm{e}^{-\pi h/d}, \tag{4}$$

where B_0 is the magnetic field in the photosphere and is taken to be 50 G (Khan *et al.*, 1998), whereas for the foot-point half-separation d we take the measured value of 8.5×10^9 cm. When $\mathrm{d}^2h/\mathrm{d}t^2 = 0$, the balance current is derived (van Tend and Kuperus, 1978) for equilibrium height $h = 0.2 \times 10^{10}$ cm. The loop length and mass of the prominence at this height are estimated to be $l = 1.9 \times 10^{10}$ cm and $m = 0.5 \times 10^{15}$ g (using a filling factor of 0.1), respectively. By using these values the strength of equilibrium current is about 1.43×10^{21} stat ampere (s.a.).

The energy stored in the prominence magnetic field is given by

$$E = \frac{1}{2}LI^2 + \frac{1}{c}\phi I, \tag{5}$$

where L is the self-inductance of the circuit and ϕ is the magnetic flux of the background field through the circuit (Martens, 1986). The calculations show that for $h \geq 5 \times 10^3$ km,

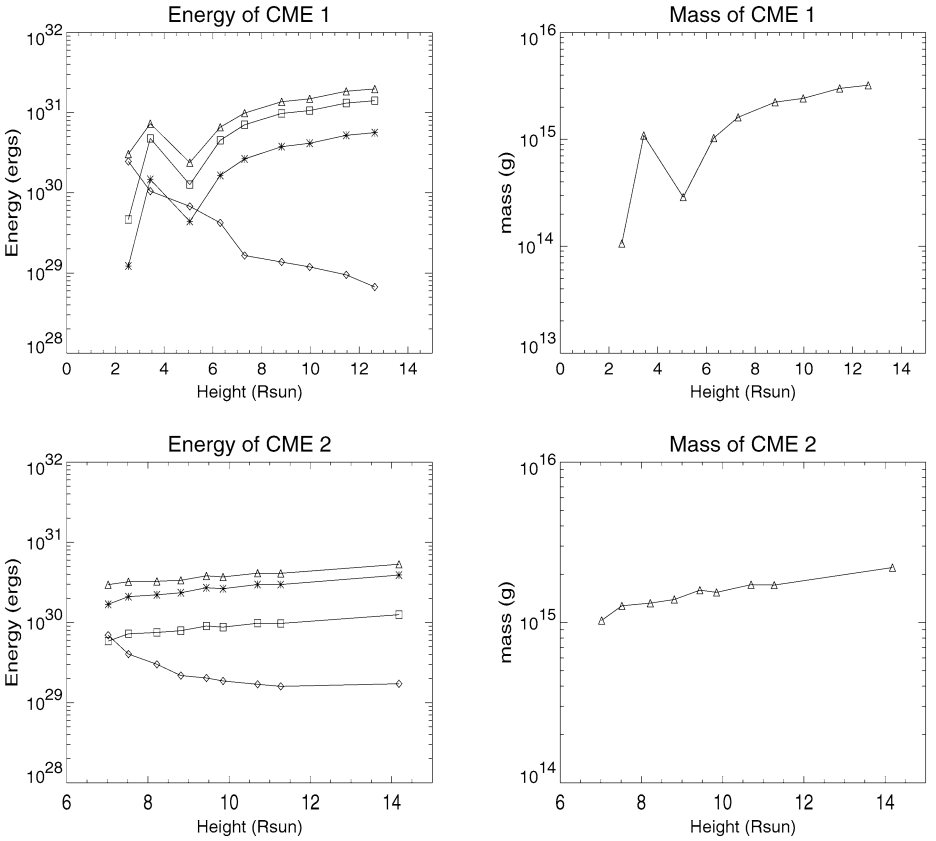

Figure 8 Left panels: Variation of potential (⋆), kinetic (□), magnetic (◇), and total (△) energy of the first and the second CME with respect to heliocentric heights. Right panels: The evolution of mass of both the CMEs as a function of their heliocentric heights.

L may be taken approximately as

$$L = \frac{2l}{c^2}(C_1 h + C_0), \tag{6}$$

where $C_0 = 1.132$ and $C_1 = 1.932$ (Martens, 1986). The unit of h is 10^4 km. According to electromagnetic theory the magnetic flux through the circuit can be written as

$$\phi = \iint B \, \mathrm{d}s = \frac{B_0 l d}{\pi}\left(1 - \mathrm{e}^{-\pi h/d}\right). \tag{7}$$

The calculations show that the energy stored in the prominence is about 2.8×10^{32} erg.

5.2. Energy of CMEs

Coronal mass ejections involve the expulsion of a huge amount of solar material into interplanetary space, at hundreds of kilometers per second. Where does this energy come from? Many CME theories invoke magnetic energy, often associated with field-aligned (force-free)

currents (*e.g.*, van Ballegooijen and Martens, 1989; Ridgeway and Priest, 1993; van Ballegooijen, 1999). Low and Smith (1993) pointed out that the amount of available energy should be sufficient to provide three things: (1) the opening of the closed magnetic field, (2) lifting the mass against gravity, and (3) driving the ejected plasma material at the observed speed. We examine the energetics of CMEs with the help of white light data taken from the LASCO C2 and C3 coronagraphs. Three forms of energies (potential, kinetic, and magnetic) are considered. The enthalpy and thermal energy are so small that they can be neglected without affecting the overall conclusions (Vourlidas *et al.*, 2000). The potential and kinetic energies are given by

$$E_{\mathrm{p}} = GM_{\mathrm{s}}m\left(\frac{1}{R_{\mathrm{s}}} - \frac{1}{R_{\mathrm{s}}+h}\right), \tag{8}$$

$$E_{\mathrm{k}} = \frac{1}{2}mv^2, \tag{9}$$

where M_{s} and R_{s} are the solar mass and radius, m and v represent the mass and velocity of the considered CME, and $R_{\mathrm{s}}+h$ is the heliocentric height of its center of mass. The average speeds of the first and the second CME are estimated to be 937 $\mathrm{km\,s^{-1}}$ and 373 $\mathrm{km\,s^{-1}}$, respectively, with the help of a linear fit to height – time data (Figure 2). The magnetic energy carried out by a CME can be expressed approximately as

$$E_{\mathrm{m}} = \frac{l}{8\pi}\frac{(B\times A)^2}{A} \tag{10}$$

(Vourlidas *et al.*, 2000), where A and l are the cross-section area and length of flux rope, respectively. For the CMEs under consideration it is difficult to identify the flux rope especially in the second CME. Hence the width of CME is taken as an indicator of the area of flux rope. We take approximately that l is equal to the heliocentric height, $l = r_{\mathrm{CME}}$. The quantity $B \times A$ is the axial magnetic flux in the rope and is considered to be conserved. We have used an average CME magnetic flux of $B \times A = 1.2 \times 10^{21}$ Mx (Wu *et al.*, 2002). For the discussion on the estimation of mass and the corresponding error estimation see Vourlidas *et al.* (2000). The variation of the potential energy (E_{p}), kinetic energy (E_{k}), magnetic energy (E_{m}), and total energy of both CMEs with their heliocentric height are shown in Figure 8. The total energies of the first and the second CME are 2×10^{31} erg and 5×10^{30} erg, respectively.

6. Discussion

It is widely believed that the prominences/filaments attain a critical twist before eruption (*e.g.*, Vršnak, 1990c; Mikić and Linker, 1994; Titov and Demoulin, 1999; Klimchuk, 2001; Török and Kliem, 2003, 2005; and references therein). In this respect, our analysis reveals three relatively unusual characteristics of the eruptive prominence of 21 April 2001:

1. The measured values of the pitch angle θ, *i.e.*, the parameter $X = \tan\theta$, fall into the stability region of the model by Vršnak (1990c). The largest measured pitch angle corresponds to $X \approx 1.2$ (Figure 6), which is around 30% smaller value than the required model value.

2. The kinematics was characterized by a quite impulsive acceleration, with a peak value of 470 $\mathrm{m\,s^{-2}}$ (Figure 3, bottom panel). Such an acceleration is difficult to explain in terms of the simple model proposed by Vršnak (1990c), even assuming an excessive drainage of material from the prominence body (see Figure 7 of Vršnak, 1990c or Figure 5a of Vršnak *et al.*, 1993).
3. The radius of the helical pattern decreased as the prominence rose (Figure 5, top panel).

As the Hα prominence is assumed to be the core of a flux rope, several possibilities could be considered to explain the strongly accelerated eruption at "subcritical" values of twist:

(i) The invisible external part of the flux rope (the cavity) may have larger values of twist.
(ii) The "injection" of flux from below the photosphere may also cause the flux rope to erupt at "subcritical" values of twist (see, *e.g.*, Figure 11b of Chen and Krall, 2003, or Table 3 of Krall *et al.*, 2001).
(iii) There might be reconnection taking place below the flux rope (*e.g.*, Kliem, Titov, and Török, 2004; Lin, Raymond, and van Ballegooijen, 2004) supplying the magnetic flux of a larger twist to the outer shell of the rope.

The first explanation does not seem likely since, as mentioned previously under item 2, even at large values of twist and excessive mass drainage, it is difficult to attain such a high acceleration without supplying an additional poloidal flux. The poloidal flux can be supplied either by the process of flux emergence (*e.g.*, Chen and Krall, 2003) or by reconnection in the current sheet below the rope (*e.g.*, Kliem, Titov, and Török, 2004; Lin, Raymond, and van Ballegooijen, 2004; Vršnak, Sudar, and Ruždjak, 2005).

Unfortunately, the former option cannot be tested observationally, since the event was observed at the limb, so there is no magnetographic information. However, we emphasize that the acceleration was very impulsive (with the main acceleration phase lasting only for some ten minutes), which would require an enormously abrupt flux emergence. Furthermore, the required amount of emerged flux at the foot-points has to be very large, usually considered to be much larger than observed (*e.g.*, Forbes, 2001). It is on the order of 10^{22} Mx (for details see, *e.g.*, Chen and Krall, 2003, and Krall *et al.*, 2001), which is comparable to a medium active region, but one should bear in mind that the injection time in the eruptive prominence of 21 April 2001 should be ten minutes only. In this respect, let us quote Wang and Sheeley (1999), who suggested that eruptions sometimes occur in the absence of any observable flux emergence and that new flux may indeed act as a strong catalyst, but it is not a necessary condition for filament/prominence destabilization.

Thus, if we abandon the interpretation in terms of the flux injection, we must either consider that some more advanced ideal MHD model has to be applied to explain the observations or include the effects of magnetic field reconnection. In this respect we recall the numerical simulations by Török and Kliem (2005), who have scaled their model of a kink-unstable flux rope to match the peak acceleration of 400 $\mathrm{m\,s^{-2}}$ in the 15 May 2001 CME (Vršnak *et al.*, 2004), which is rather close to the value obtained here. The same simulation was scaled to an extremely fast CME on 10 November 2004 (Williams *et al.*, 2005), to match an acceleration of about 9 000 $\mathrm{m\,s^{-2}}$ at the final data point. Both the ideal MHD instability and magnetic reconnection were found to contribute substantially in the simulated dynamics of eruption.

In the context of reconnection, let us also discuss the decrease of the radius of the helical pattern mentioned previously in item 3. Such a situation can be found in the model by Vršnak (1990b, 1990c), where it was shown that the flux-rope radius decreases if the axial current is kept constant, *i.e.*, when the current is considered as a part of the global current system.

However, in such a case the energy LI^2 of the prominence structure would be increasing, since the inductivity L is proportional to the size of the structure (*e.g.*, Chen and Krall, 2003; Vršnak *et al.*, 2004). Thus, a more probable explanation is that the inward magnetic tension of the poloidal magnetic field associated with the reconnected field lines that are wrapped around the flux rope core could cause the compression of the inner parts of the rope where the prominence was located.[2] However, the eruption models that are based on the reconnection below the flux rope (*e.g.*, Lin and Forbes, 2000, or Lin, Raymond, and van Ballegooijen, 2004) usually do not show such an effect.

The main drawback of the interpretation in terms of reconnection is that we found no flare signature associated with this eruption; *i.e.*, there was no X-ray, microwave, or radio burst recorded. However, one should bear in mind the fact that reconnection does not necessarily result in strong plasma heating or particle acceleration. Studies of the disappearing filaments have shown nice examples where reconnection does take place, but without any significant flare-like emission (Schmieder, Golub, and Antiochos, 1994; Cane, Kahler, and Sheeley, 1986; Kahler *et al.*, 1986; Forbes, 2000). It usually happens when the prominence/filament eruption takes place outside the active region. In such an environment the plasma-to-magnetic pressure ratio is higher than in active regions, which implies that the reconnection associated with such events is likely to produce only a weak heating (Skender, Vršnak, and Martenis, 2003; Vršnak and Skender, 2005).

7. Summary

The study of geometrical parameters of the eruptive prominence of 21 April 2001 reveals that the prominence has erupted although its twist falls into the stability region of the ideal MHD model by Vršnak (1990c). We proposed several possible explanations, and in our opinion the most likely one is that magnetic reconnection played a substantial role in the dynamics of the eruption. In comparison to pure MHD models, the models that include reconnection — the breakout model (Antiochos, 1998; Antiochos, De Vore, and Klimchuk, 1999), the flux rope model (Forbes and Isenberg, 1991; Amari, Luciani, and Linker, 2000; Wu *et al.*, 2000; Török and Kliem, 2005), or the tether cutting model (Sturrock *et al.*, 1984; Moore *et al.*, 2001) — seem to be better suited to deal with the complex eruptions like the present one.

Our observations show the well-known three-part structure of CMEs (Illing and Hundhausen, 1986): a bright leading edge, a dark cavity, and a bright core (prominence). The spatial and temporal correlation between CME and prominence eruption is found to be good. Since there was no flare or radio burst associated with the eruption, our analysis supports the idea that neither radio bursts nor flares are necessary for CME production though generally they have good association with CMEs. A similar conclusion has been drawn for the CME of 5 December 1981 (Cane, Kahler, and Sheeley, 1986; Kahler *et al.*, 1986) and for the CME of 6 January 1997 (Wu *et al.*, 2002). We have shown that the energy stored in the prominence (2.8×10^{32} erg) is sufficient to power both associated CMEs (the combined energy of both the CMEs being 2.5×10^{31} erg). From Figure 8 it is clear that the total energy of both CMEs is roughly constant within a factor of 2 and the potential energy increases at the expense of magnetic energy. The decrease in magnetic

[2]Note that a similar effect, *i.e.*, the aspect ratio increase, is expected also in the case of the poloidal flux injection at the foot-points (see, *e.g.*, Figure 6 of Krall *et al.*, 2001).

energy is a direct consequence of CME expansion, thus indicating that the CMEs are magnetically driven and internally powered (Vourlidas *et al.*, 2000; Manoharan *et al.*, 2001; Ali, Uddin, and Chandra, 2006).

Acknowledgements We express our sincere thanks to Dr. Angelos Vourlidas of the Naval Research Laboratory, Washington, DC, for his help and inspiring discussions, as well as to Dr. Bernhard Kliem (the referee), whose comprehensive review of the manuscript helped us very much in improving the paper. We are also grateful to Prof. Ram Sagar, Director of ARIES, for extending every possible help at his disposal to carry out the present study. Thanks are also due to the Vice-Chancellor, Aligarh Muslim University, Aligarh, for granting leave to pursue the present study. The open data policy of SOHO is thankfully acknowledged.

Appendix

From the Hα data, the positions of the leading edge of the prominence at different times, $R_i(t_i)$, were measured and then smoothed using cubic splines. The smoothing procedure is similar to that described in Maričić *et al.* (2004). From the smoothed data $\hat{R}(\hat{t})$, the velocities $\hat{v}(\hat{t})$ were evaluated by taking two successive smoothed data points:

$$\hat{v}(\hat{t}_j^v) = \frac{\hat{R}(\hat{t}_{j+1}) - \hat{R}(\hat{t}_j)}{\hat{t}_{j+1} - \hat{t}_j} r_s, \tag{11}$$

where $\hat{R}(\hat{t}_j)$ is the smoothed radial distance at time $\hat{t}_j$, and $\hat{t}_j^v = (\hat{t}_{j+1} + \hat{t}_j)/2$. In the next step, similarly the acceleration was estimated as

$$\hat{a}(t_j^a) = \frac{\hat{v}(t_{j+1}^v) - \hat{v}(t_j^v)}{t_{j+1}^v - t_j^v}, \tag{12}$$

where $t_j^a = (t_{j+1}^v + t_j^v)/2$.

An important issue in the smoothing procedure is to quantify how much the results obtained for the velocity and acceleration depend on the smoothing parameters. These parameters are the degree of the smoothing spline and the weights given to the knots. A higher degree in the smoothing spline results in a fit closer to the data and, in turn, in a noisier acceleration. A lower spline degree results in a smoother fit, but may underestimate the value of the acceleration amplitude. The weights of the knots determine how the data points are accounted for in the smoothing procedure. Larger weights are attributed to reliable points, and smaller weights to less reliable (noisy) points.

The degree of the smoothing spline was chosen in such a manner to have both a reasonably smooth acceleration profile and an accurate estimation of the amplitude. Then, three intervals were distinguished in the raw data $R_i(t_i)$ (top panel of Figure 3). The first and third intervals (0 – 100 s and 600 – 800 s, respectively) correspond to data for which the position of the leading edge could be most accurately estimated. During the acceleration phase, the fast motion of the leading edge made the estimation of the position of the leading edge in the images more difficult. For this reason, the corresponding data points (second interval, 200 – 600 s) exhibit a somewhat steplike shape. Because these points can be considered as less accurate, they were attributed smaller weights in the smoothing. The smoothed heights, velocities, and acceleration are plotted in Figure 3.

While investigating the influence of the parameters in the smoothed profiles, it turned out that an important factor is the weights attributed to the position data points in the transition region between intervals 1 and 2. Two extreme smoothing options, corresponding to a sharp

and a blunt acceleration profile, were applied. These two extreme profiles were used to select the correct acceleration profile (*i.e.*, that of Figure 3, which is in the parameter space at equal distance of the two extreme profiles) and to derive the error bars in the kinematic quantities estimated from the smoothing. On the basis of our investigation of the parameter space, our opinion is that the maximum acceleration is in fact accurate to, say, 10 $\mathrm{m\,s^{-2}}$, because most of the smoothing strategies result in acceleration profiles similar to that of Figure 3. However, we cannot exclude larger deviations (up to 70 $\mathrm{m\,s^{-2}}$) from the adopted value of 470 $\mathrm{m\,s^{-2}}$.

References

Ali, S.S., Uddin, W., Chandra, R.: 2006, *J. Astrophys. Astron.* **27**, 347.
Amari, T., Luciani, J.F., Linker, J.: 2000, *Astrophys. J.* **529**, L49.
An, Ch.-H.: 1984, *Astrophys. J.* **281**, 419.
Antiochos, S.K.: 1998, *Astrophys. J.* **502**, L181.
Antiochos, S.K., De Vore, C.R., Klimchuk, J.A.: 1999, *Astrophys. J.* **510**, 485.
Brueckner, G., *et al.*: 1995, *Solar Phys.* **162**, 357.
Cane, H.V., Kahler, S.W., Sheeley, N.R., Jr.: 1986, *J. Geophys. Res.* **91**, 13321.
Chen, J., Krall, J.: 2003, *J. Geophys. Res.* **108**(A11), 1410.
Delaboudiniere, J.P., *et al.*: 1995, *Solar Phys.* **162**, 291.
Engvold, O., Malville, J.M., Rustad, B.M.: 1976, *Solar Phys.* **48**, 137.
Filippov, B.P.: 1998, In: Rust, D., Webb, D.F., Schmieder, B. (eds.) *New Perspective on Solar Prominences, IAU Colloq.* **167**, 342.
Forbes, T.G.: 2000, *J. Geophys. Res.* **105**, 23153.
Forbes, T.G.: 2001, *EOS* **82**(20), SH41C-03.
Forbes T.G., Isenberg P.A.: 1991, *Astrophys. J.* **373**, 294.
Gopalswamy, N., Shimojo, M., Lu, W., Yashiro, S., Shibasaki, K., Howard, R.A.: 2003, *Astrophys. J.* **586**, 562.
Hood, A., Anzer, U.: 1987, *Solar Phys.* **111**, 333.
House, L.L., Berger, M.A.: 1987, *Astrophys. J.* **323**, 406.
Hundhausen, A.J.: 1999, In: Strong, K.T., Saba, J.L., Haisch, B.M., Schmelz, J.T. (eds.) *The Many Faces of the Sun*, Springer, New York, 143.
Illing, R.M., Hundhausen, A.J.: 1986, *J. Geophys. Res.* **91**, 10951.
Joshi, A., Chandra, R., Uddin, W.: 2003, *Solar Phys.* **217**, 173.
Kahler, S.W., Cliver, E.N., Cane, H.V., Mc Guire, R.E., Stone, R.G., Sheeley, N.R., Jr.: 1986, *Astrophys. J.* **302**, 504.
Khan, J.I., *et al.*: 1998, *Astron. Astrophys.* **336**, 753.
Klimchuk, J.A.: 2001, In: Song, P., Singer, H.J., Siscoe, G.L. (eds.) *Space Weather*, *Geophysical Monograph* **125**, American Geophysical Union, 143.
Kliem, B., Titov, V.S., Török, T.: 2004, *Astron. Astrophys.* **413**, L23.
Krall, J., Chen, J., Duffin, R.T., Howard, R.A., Thompson, B.J.: 2001, *Astrophys. J.* **562**, 1045.
Kuperus, M., Raadu, M.A.: 1974, *Astron. Astrophys.* **31**, 189.
Lin, J., Forbes, T.G.: 2000, *J. Geophys. Res.* **105**, 2375.
Lin, J., Raymond, J.C., van Ballegooijen, A.A.: 2004, *Astrophys. J.* **602**, 422.
Low, B.C.: 1996, *Solar Phys.* **167**, 217.
Low, B.C., Smith, D.F.: 1993, *Astrophys. J.* **410**, 412.
Manoharan, P.K., *et al.*: 2001, *Astrophys. J.* **559**, 1180.
Maričić, D., Vršnak, B., Stanger, A.L., Veronig, A.: 2004, *Solar Phys.* **225**, 337.
Martens, P.C.H.: 1986, *Solar Phys.* **107**, 95.
Martens, P.C.H., Kuin, N.P.M.: 1989, *Solar Phys.* **122**, 263.
Mikić, Z., Linker, J.A.: 1994, *Astrophys. J.* **430**, 898.
Moore, R.L.: 1988, *Astrophys. J.* **324**, 1132.
Moore, R.L., Sterling, A.C., Hudson, H.S., Lemen, J.R.: 2001, *Astrophys. J.* **552**, 833.
Munro, R.H. *et al.*: 1979, *Solar Phys.* **61**, 201.
Pneuman, G.W.: 1980, *Solar Phys.* **65**, 369.
Priest, E.R.: 1985, *Prog. Rep. Phys.* **48**, 955.
Priest, E.R., Hood, A.W., Anzer, U.: 1989, *Astrophys. J.* **344**, 1010.

Priest, E.R., Krishnan, V.: 1990, *Basic Plasma Processes on the Sun*, Kluwer Academic, Dordrecht, p. 293.
Ridgeway, C., Priest, E.R.: 1993, *Solar Phys.* **146**, 277.
Romano, P., Contarino, L., Zuccarello, F.: 2003, *Solar Phys.* **214**, 313.
Sakurai, T.: 1976, *Publ. Astron. Soc. Japan* **28**, 177.
Schmieder, B.: 1990, In: Ruždjak, V., Tandberg-Hanssen, E. (eds.) *Dynamics of Quiescent Prominences*, *Lecture Notes in Physics* **363**, Springer-Verlag, Berlin, 85.
Schmieder, B., Golub, L., Antiochos, S.K.: 1994, *Astrophys. J.* **425**, 326.
Skender, M., Vršnak, B., Martenis, M.: 2003, *Phys. Rev. E* **68**, 046405.
Smith, D.F., Hildner, E., Quin, N.P.M.: 1992, *Solar Phys.* **194**, 371.
St. Cyr, O., Webb, D.F.: 1991, *Solar Phys.* **137**, 317.
Sturrock, P.A., Kaufman, P., Moore, R.L., Smith, D.F.: 1984, *Solar Phys.* **94**, 341.
Tandberg-Hanssen, E.: 1995, *The Nature of Solar Prominences*, Kluwer Academic, Dordrecht.
Tandberg-Hanssen, E. Malville, J.M.: 1974, *Solar Phys.* **39**, 107.
Tang, Y.H., *et al.*: 1999, *Solar Phys.* **185**, 143.
Titov, V.S., Demoulin, P.: 1999, *Astron. Astrophys.* **351**, 701.
Török, T., Kliem, B.: 2003, *Astron. Astrophys.* **406**, 1043.
Török, T., Kliem, B.: 2005, *Astrophys. J.* **630**, L97.
Uchida, Y.: 1974, *Solar Phys.* **39**, 431.
van Ballegooijen, A.A.: 1999, In: Brown, M.R., Canfield, R.C., Pestov, A.A. (eds.) *Magnetic Helicity in Space and Laboratory Plasmas*, *Geophysical Monograph* **111**, 213.
van Ballegooijen, A.A., Martens, P.C.H.: 1989, *Astrophys. J.* **343**, 971.
van Tend, W., Kuperus, M.: 1978, *Solar Phys.* **59**, 115.
Vourlidas, A., Subramanian, P., Dere, K.P., Howard, R.A.: 2000, *Astrophys. J.* **534**, 456.
Vršnak, B.: 1988, *Solar Phys.* **116**, 45.
Vršnak, B.: 1990a, *Solar Phys.* **127**, 129.
Vršnak, B.: 1990b, *Astrophys. Space Sci.* **170**, 141.
Vršnak, B.: 1990c, *Solar Phys.* **129**, 295.
Vršnak, B., Maričić, D., Stanger, A.L., Veronig, A.: 2004, *Solar Phys.* **225**, 355.
Vršnak, B., Ruždjak, V., Rompolt, B.: 1991, *Solar Phys.* **136**, 151.
Vršnak, B., Ruždjak, V., Rompolt, B., Rosa, D., Zlobec, P.: 1993, *Solar Phys.* **146**, 147.
Vršnak, B., Skender, M.: 2005, *Solar Phys.* **226**, 97.
Vršnak, B., Sudar, D., Ruždjak, D.: 2005, *Astron. Astrophys.* **435**, 1149.
Wang, Y.-M., Sheeley, N.R., Jr.: 1999, *Astrophys. J.* **510**, 157.
Webb, D.F., Hundhausen, A.J.: 1987, *Solar Phys.* **108**, 383.
Webb, D.F., Krieger, A.S., Rust, D.M.: 1976, *Solar Phys.* **48**, 159.
Williams, D.R., Török, T., Dcmoulin, P., van Driel-Gesztelyi, L., Kliem, B.: 2005, *Astrophys. J.* **628**, L163.
Wu, S.T., Guo, W.P., Plunkett, S.P., Schmieder, B., Simnett, G.M.: 2000, *J. Atmos. Solar-Terr. Phys.* **62**, 1489.
Wu, Y.Q., Tang, Y.H., Di, Y., Wu, G.P.: 2002, *Solar Phys.* **207**, 159.